published in: Material Science and Engineering A, Vol. 489 (2008) 138–149

Age hardening and softening in cold-rolled Al-Mg-Mn alloys with up to 0.4wt%Cu

Z. Zhu, M.J. Starink

Materials Research Group, School of Engineering Sciences, University of Southampton, Southampton S017 1BJ, UK

Abstract

The age hardening and age softening of nine solution treated and subsequently cold-rolled Al-(1-3)Mg-(0-0.4)Cu-0.15Si-0.25Mn (in wt%) alloys with potential applications in both packaging and automotive industries have been investigated. Cold work levels were 10, 40 and 90% reduction. The proof strengths of the aged alloys range from 130 to 370MPa. A physically based model for yield strength has been developed which includes a one parameter dislocation evolution model to describe work hardening and recovery and a two precipitate precipitation hardening model. The model is based on analytical equations, avoiding computing time intensive iterative schemes. An exceptionally high model accuracy has been demonstrated. The model parameters are verified by transmission electron microscopy and calorimetry analysis of the materials.

1. Introduction

The main strengthening mechanisms in aluminium alloys are work hardening, solution strengthening and precipitation strengthening, and in many cases one of these mechanisms is dominant. In most applications of Al-Mn based (3XXX) and Al-Mg based (5XXX) alloys both work hardening and solution strengthening are important contributors, and small Cu additions can improve the strength due to some limited precipitation hardening. These types of alloys have been widely used in beverage cans for decades [1], and aluminium alloys are increasingly being used as car body panels to reduce weight and thus improve fuel economy and emissions [2]. For this application 5XXX with Cu additions are very promising candidates for these applications because of their excellent formability, good strength and the benefits of precipitation hardening during paint-baking due to Cu additions [3,4,5].

The alloys used for the above-mentioned canstock and automotive applications are generally warm or cold rolled to achieve thin gauge. During the processing of alloys with Cu additions, precipitation of strengthening phases occurs during hot and cold rolling as well as during heat treatment after cold rolling [6]. In both cases, precipitation will change the yield stress and the work hardening, which will affect subsequent further working of the alloys. In the case of beverage can applications, the cold rolled alloys are used in a work hardened condition, but for the car body application, they will be supplied to car manufacturers with O temper (annealed) due to the higher requirement of excellent formability during car body forming. For both applications, a further elevated temperature

process in the form of coating/painting and baking are needed. Both recovery and precipitation will occur during these processes.

From the above it will be apparent that understanding of the composition-processing-property relations in Al-Mg-Mn based alloys with Cu additions is important. In the present paper we will present data on the strength of nine cold rolled and subsequently aged Al-Mg-Mn alloys with up to 0.4wt%Cu. The strength will be analysed, and a physically based model for the strength will be presented.

Physically-based models of strength development in precipitation hardening alloys have been constructed using a range of approaches. The main elements in such models are the description of the thermodynamics (equilibrium and metastable equilibrium), the kinetics of transformations and the relation between strength and microstructure, which is determined by the interaction between dislocations and elements in the microstructure. For each of these three main elements different approaches have been applied. For instance, modelling of the kinetics of precipitation reactions has been pursued using methods which can be divided into three broad groups. In the most computationally intensive method entire diffusion fields around growing precipitates are calculated. This modelling strategy can potentially provide the greatest level of detail, allowing explicit introduction of such quantities as local composition-dependent free energies, local interfacial energies and 3D local strain fields. The ever increasing availability of supercomputers is favouring this strategy. At present, however, most models that combine precipitation modelling with a prediction of one or more mechanical property (such as yield strength) apply more computationally efficient models such as the Johnson-Mehl-Avrami-Kolmogorov (JMAK) type treatments (see e.g. [7] and references therein) or Kampmann-Wagner (KW) type models [8]. In the present work we will present a model for microstructure evolution and yield strength, in which the reaction kinetics component derives from concepts related to the JMAK approach. The model is tested against a large amount of data: about 100 yield strength values for the nine alloys covering a range of cold working reductions and ageing treatments are reported. The model will be critically tested through model predictions for ‘unseen’ data, i.e. data that has not been used in model calibration.

2 Experimental.

In this study, nine Al-(1-3)Mg-(0-0.4)Cu-Mn alloys (in wt%) were investigated; their compositions are shown in Table 1. The alloys were produced at the former Alcan Banbury Labs, Banbury, UK. All alloys were direct chill (DC) cast. The cast ingots were preheated and homogenised at 540ºC, and subsequently hot rolled down to 5 mm in thickness. After that, the hot rolled sheets were solution treated at 500ºC for 20 minutes, followed by cold rolling to 10%, 40% and 90% reduction. Transmission electron microscopy and electron backscatter diffraction studies of the as cold-rolled material were reported elsewhere [9].

Table 1 Compositions of the alloys studied (in wt%)

Alloy No.	Mg	Cu	Mn	Fe	Si	Al
A1	1.02	<.01	0.25	0.22	0.16	
A2	1.96	<.01	0.25	0.20	0.15	
A3	2.95	<.01	0.24	0.20	0.15	
A4	1.01	0.18	0.26	0.21	0.14	
A5	1.91	0.18	0.25	0.19	0.14	bal.
A6	2.99	0.19	0.24	0.19	0.15	
A7	1.03	0.39	0.26	0.20	0.14	
A8	1.98	0.39	0.25	0.21	0.15	
A9	2.9	0.4	0.25	0.19	0.15	

The tensile testing specimens were designed based on and within the specification of the ASTM-E8M standard. To ensure that fracture takes place close to the centre of the samples, a small and gradual change in the cross sectional area of about 0.8% such that the minimum cross sectional area is located in the middle of the gauge length of the sample. The tensile axis is taken in the longitudinal (L) direction (i.e. the rolling direction). Tensile testing was performed for cold worked and cold worked-and-aged samples. For the latter test samples had been isothermally aged at 170°C in an oven. For each condition usually two tests were performed. Tensile tests were performed using an 8800 series Instron machine at a constant strain rate of 0.001 s^{-1}.

For hardness tests, samples were isothermally aged at 170°C in an oven. Hardness tests were performed using a micro-Vickers hardness tester with 1 kg load held for 15s. The mean of 5 indentations was taken as the hardness of the corresponding condition.

For analyses by differential scanning calorimetry (DSC), small disks were prepared. The DSC experiments were conducted in a Perkin-Elmer Pyris 1 DSC. All experiments were run at a constant heating rate of 10ºC/min. Details and methodology for DSC experiments and baseline correction are provided elsewhere [10].

3 Results.

Fig. 1 shows the hardness evolution during isothermal ageing at 170°C for samples after solutionising at 500°C and subsequent cold rolling with 90%, 40% and 10% reductions. Fig. 1 shows that for all cold rolling reductions, the Cu-containing alloys precipitation harden during ageing at 170°C. (The occasional absence of a distinct hardening effect for some alloy/reduction combination might be due to the interactions between recovery and precipitation and/or measurement errors.) But for Cu free alloys, the hardening response becomes slightly more complicated. For all three reductions, the Cu free alloy A1 shows a distinct precipitation hardening

effect. The hardening effect in this alloy during ageing is thought to be due to precipitation hardening due to the β″/β′/β (Mg_2Si) precipitation sequence [5].

a.

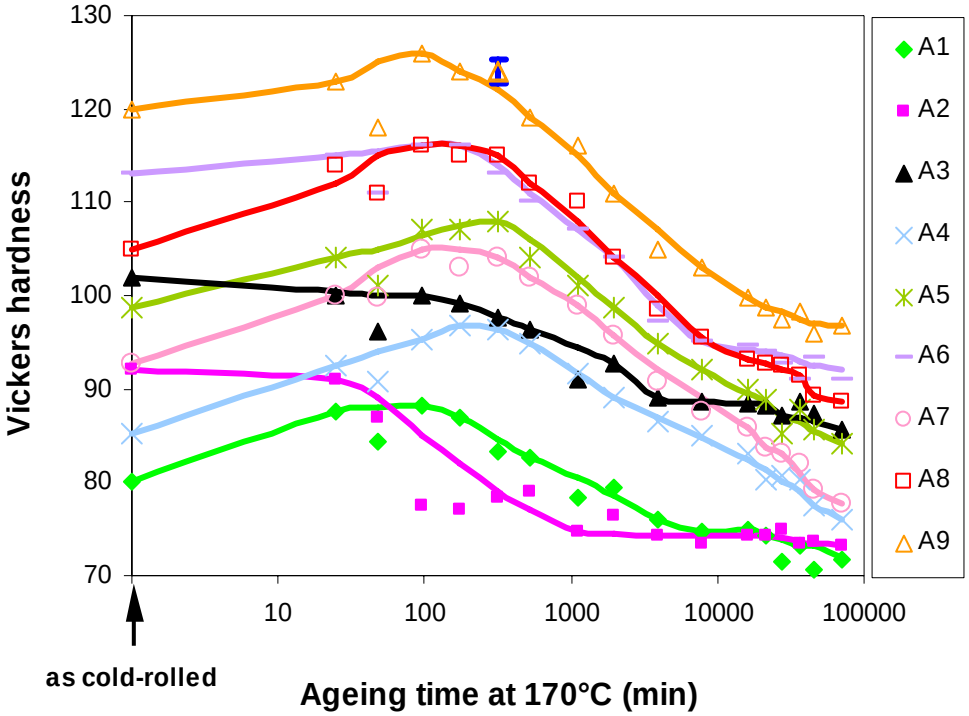

b.

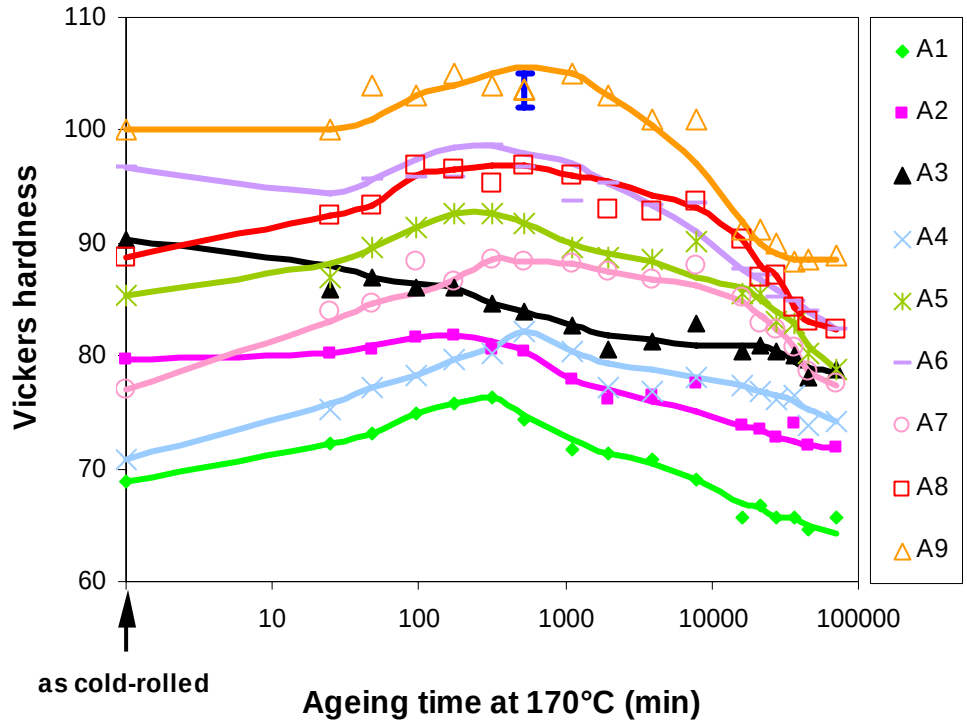

c.

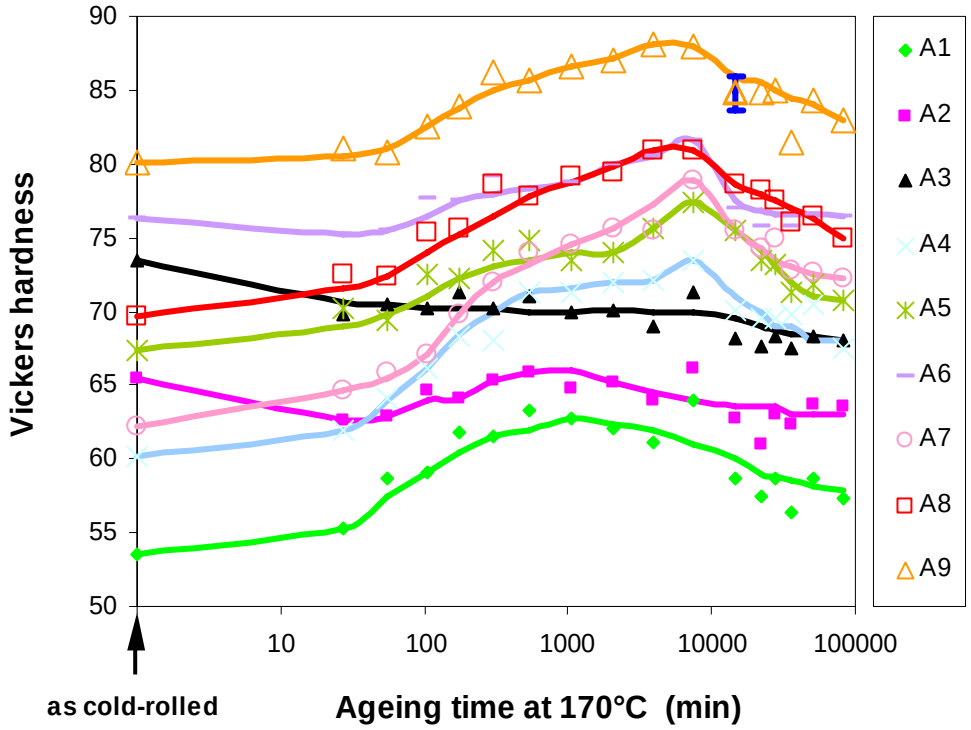

Fig. 1 Hardness during isothermal ageing at 170ºC for cold worked samples with : a. 90% reduction; b. 40% reduction; c. 10% reduction.

The hardness increases with cold rolling reduction, but on extensive ageing the differences in the hardness due to different cold-rolling reductions become smaller. On the other hand, for age hardening alloys, the time to peak hardness of each alloy decreases with increasing cold rolling reduction. For Cu-containing alloys, it takes about 2 hours, 4 hours and 5 days to reach a peak hardness for 90%, 40% and 10% reductions, respectively. But for Cu-free alloy A1, it takes about 1 hours, 4 hours and 16 hours to reach a peak hardness for 90%, 40% and 10% reductions, respectively. This difference is thought to be due to the difference in the type of precipitates responsible for peak hardness. The accelerated age hardening with increasing cold rolling reduction is thought to be due to the enhanced dislocation density which provides more heterogeneous nucleation sites for precipitation.

For each alloy/cold work combination, tensile tests were conducted for four conditions: as-cold worked, underaged, near peak aged and overaged conditions. Results are presented in Fig. 2. (The lines in this figure are model predictions, which are introduced and discussed in subsequent sections.) Tensile tests were also conducted on the solution treated alloys (without cold work) to evaluate the solution strengthening contribution due to Mg and Cu, this work is presented elsewhere [5]. The general trends in the evolution of the 0.2% proof strength, $\sigma_{0.2}$, on ageing for the nine alloys (Fig. 2) are generally consistent with the observations of the hardness development of these alloys during ageing (Fig. 1).

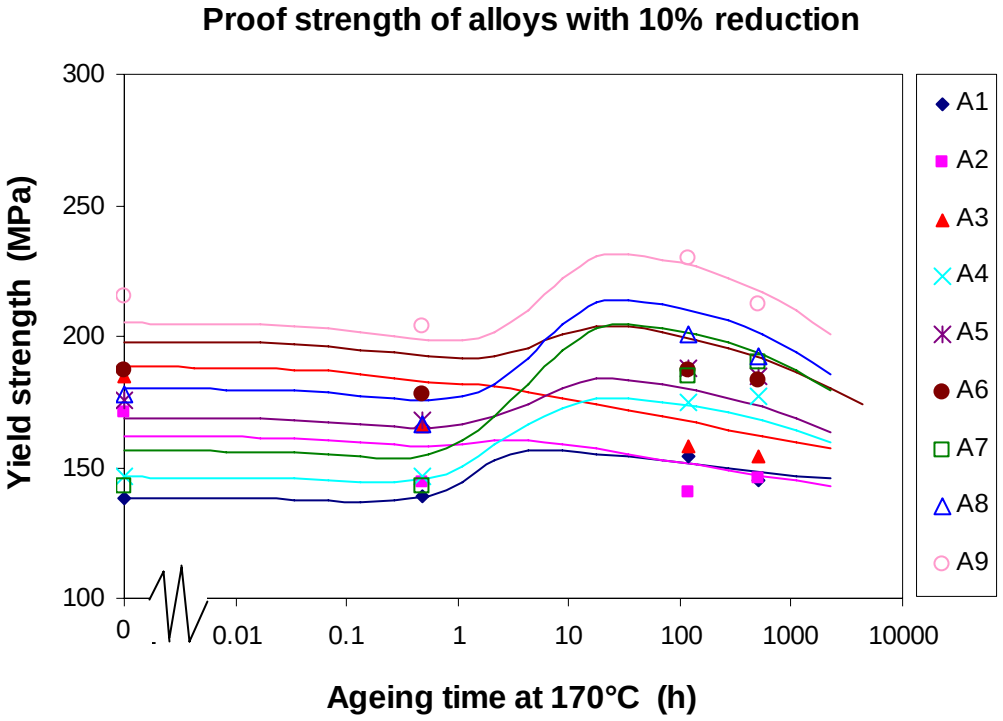
Proof strength of alloys with 10% reduction
Yield strength (MPa)
300
250
200
150
100
0
0.01
0.1
1
10
100
1000
10000
Ageing time at 170°C (h)
A1
A2
A3
A4
A5
A6
A7
A8
A9

a.

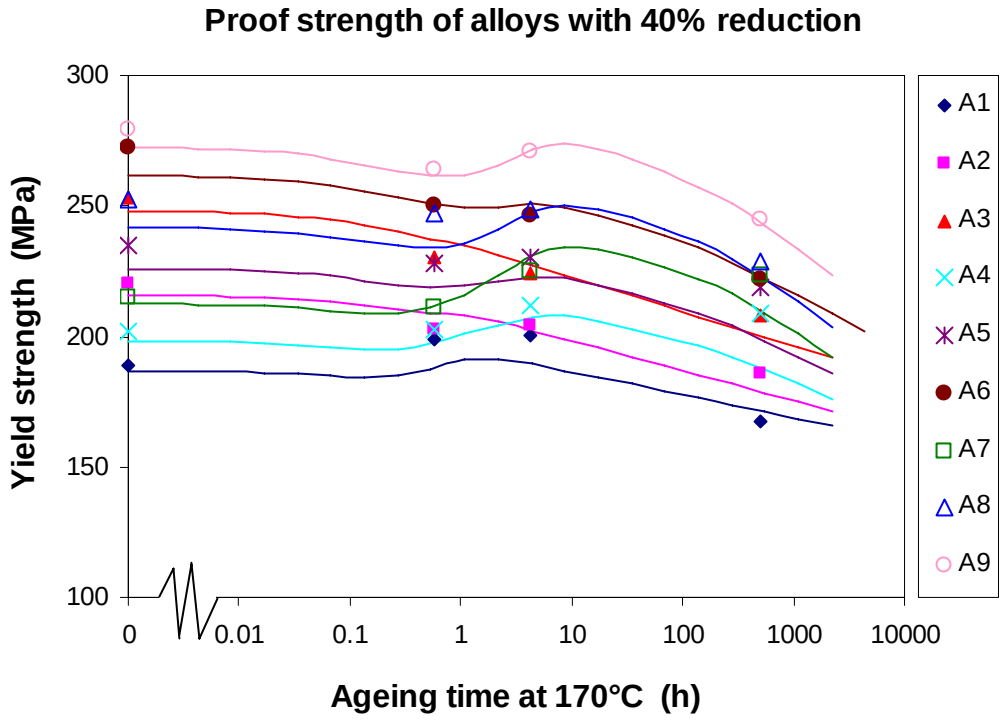
Proof strength of alloys with 40% reduction
Yield strength (MPa)
300
250
200
150
100
0
0.01
0.1
1
10
100
1000
10000
Ageing time at 170°C (h)
A1
A2
A3
A4
A5
A6
A7
A8
A9

b.

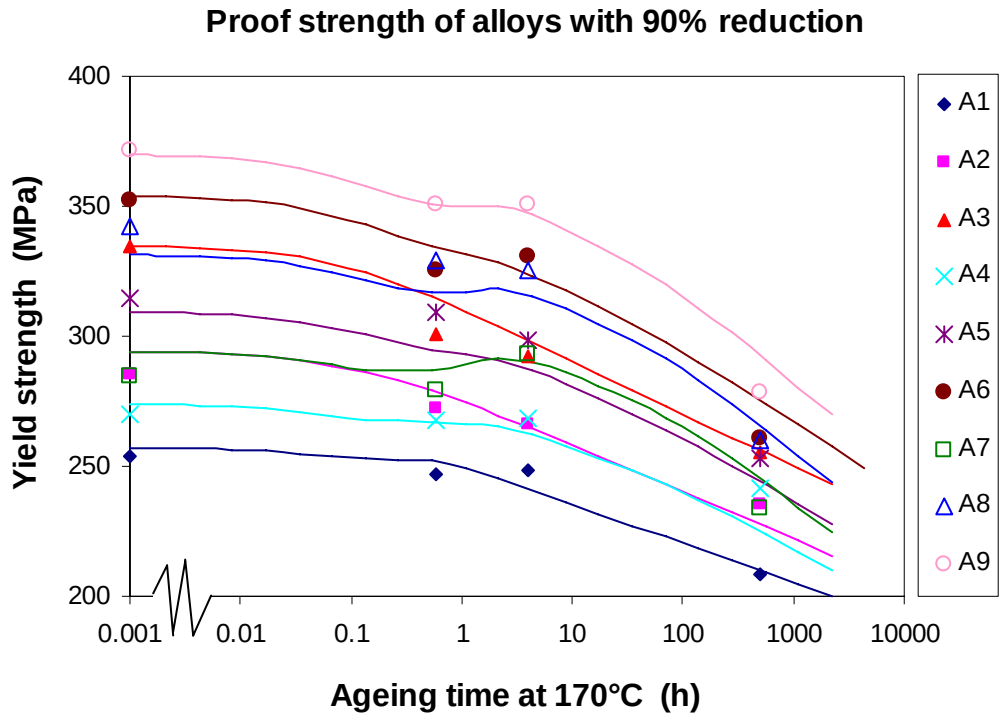

c.

Fig. 2 Yield strength vs. ageing time at 170ºC for cold-worked and subsequently aged samples: a. 10% cold work; b. 40% cold work; c. 90% cold work (The solid lines in the figure are the predictions using the model developed in this study).

Analysis of $\sigma_{0.2}$ in as cold worked condition shows that $\sigma_{0.2}$ increases approximately linearly with Mg content regardless of the level of cold work (Fig. 3). As shown in Fig. 3, the strength increment due to Mg addition also increases with increasing level of cold work: there is a synergistic effect of Mg addition and cold work. For Cu content, the yield strength increases with Cu content at higher level of cold work, e.g., 40% and 90%, but such trend is not evident at a lower level of cold work (see Fig. 3).

4 Model for age hardening and softening.

In the present section we will develop a model that will be used to fit the proof strength during age hardening and softening of the alloys and, more importantly, provide a predictive model for proof strength during age hardening and softening of any alloy with similar composition. Several elements of the thermodynamics and precipitation model have been described in detail in previous publications [7,10,11,12,13,14,15], where these elements were used in models for Al-Cu-Mg and Al-Zn-Mg-Cu alloys. In order to avoid repetition we will here refer to previous papers for most justifications and derivations. It is relevant to note that we will often use a simplified view of the relevant mechanism, and that in most elements of the model a wide range of refinements are possible. The aim of the work however is to demonstrate that an exceptionally high accuracy in predicting proof stress can be obtained using the present formulation based on analytical equations.

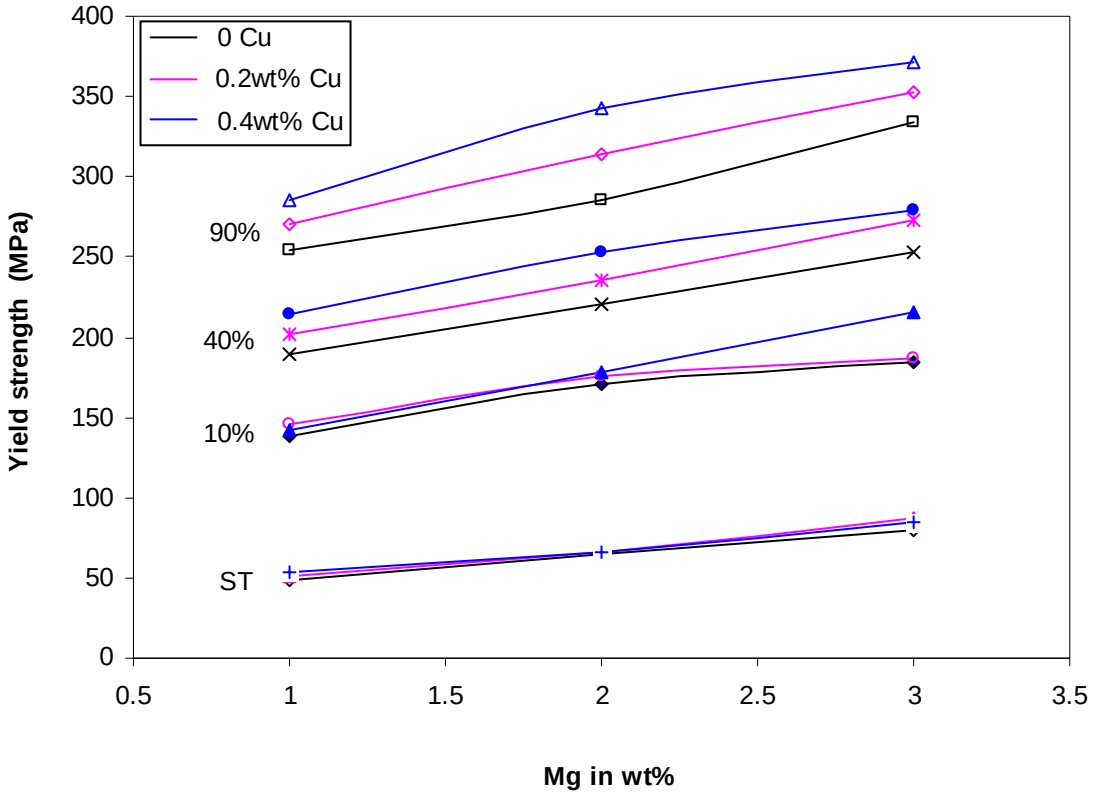

Fig. 3 Yield strength ($\sigma_{0.2}$) at different cold work levels vs. Mg and Cu contents. Lines are added as guide only

4.2 Precipitation model

The phase constitution and precipitation sequences in these alloys are complicated, and depend on the alloy's composition and pre-strains. In the present precipitation model the following simplifying assumptions were used:

1. At the ageing temperature considered, no clusters/zones (see e.g. [16]) form during artificial ageing of the cold-worked alloys.
2. The model is limited to considering two precipitates. These are the precipitate responsible for peak strength in Al-Si-Mg based alloys, β″ phase [17,18,19], and the precipitate responsible for peak strength in Al-Cu-Mg based alloys, S phase [15,20,21,22]. In support it is noted that quaternary Al-Mg-Si-Cu precipitates (see e.g. [23]) have not been reported for the present types of alloys with very low Cu and Si contents; whilst Mg contents are too low to allow precipitation of binary Al-Mg precipitates [24].
3. S and β″ phase have fixed stoichiometries of Al_2CuMg and Mg_2Si, respectively.

The components of the precipitation model include a thermodynamic model for prediction of the solvi boundaries for the relevant phases and a kinetic model for prediction of the fraction transformed, the average precipitate size and volume fraction of precipitates (S and β″) as a function of alloy composition, ageing temperature, time and pre-strain (i.e. cold rolling reduction).

Thermodynamic model

Various types of thermodynamic models can be used in age hardening models. As we are here concerned with a model that can be formulated in analytical equations, we have opted to formulate the thermodynamic model in the form of a regular solution model. In this model, each phase is considered to have a fixed stoichiometry of $M_mA_aB_b$ (M is the main constituent of the alloy and A, B are the alloying elements). Hence the solvi of the β phase (which can remain partly undissolved during solution treatment), and the precipitating S and β″ phases are given by [14]:

$$(c_e^A)^a (c_e^B)^b = \Delta S_i \exp(-\frac{\Delta H^i}{RT}) \quad (1)$$

where ΔH^i is the formation enthalpy per unit of phase i, c_e^A and c_e^B are the solubilities of alloying elements *A* and *B* (in atomic fraction), respectively, and ΔS_i is an entropy term which is assumed to be constant. Intermetallic phases $Al_{12}(Fe,Mn)_3Si$ and $Al_6(Fe,Mn)$ can occur, but do not contribute significantly to strengthening and do not significantly alter the availability of dissolved atoms relevant for precipitation hardening [5]. Hence they are not included in the model.

Kinetic model: precipitate volumes

Following the Starink-Zahra (SZ) model [7], the fraction transformed for a phase i during isothermal ageing can be expressed as:

$$\alpha_i(T,t) = 1 - \left(\frac{[k_i(T,\varepsilon)t]^{n_i}}{\eta} + 1 \right)^{-\eta} \quad (2)$$

where n_i are the reaction exponents (or Avrami exponent) for the precipitation of phase i (e.g. S or β″), η is the impingement exponent, $k_i(T,\varepsilon)$ are the temperature and pre-strain dependent factor for the formation of phase i (S or β″). They are given in an Arrhenius form as follows:

$$k_i(T,\varepsilon) = k_{0,i}(\varepsilon) \exp(-\frac{E^i_{ppt}}{RT}) \quad (3)$$

where E^i_{ppt} are the activation energy for the precipitation reaction of phase i. $k_{0,i}(\varepsilon)$ are pre-exponential factors for the precipitation of phase i, which depends on the pre-strain, ε, of the alloy subjected to during cold work before ageing.

Several of the parameters appearing in the latter two equations can be obtained from data and model analysis in earlier work by Starink and co-workers [7,10,11,12,25]. Following earlier work on S phase formation [11,12,25] n_S is taken as 2.5 throughout the model; this value is valid for reaction which involve continuous nucleation and diffusion controlled growth in 3 dimensions [7,10]. β″

formation is thought to also occur by continuous nucleation and diffusion controlled growth in 3 dimensions and hence n_β is taken to be identical [26]. Earlier work [7,10] has shown that η_i =1 is an appropriate choice for most precipitation reactions, and it has specifically been validated for S phase formation [11,25]. Hence this value is adopted throughout this study. In this work we will only consider data on ageing at a single temperature and hence the activation energies for the processes will not be tested. (We will set the activation energies for precipitation and coarsening equal to the activation energy for S phase formation, which is 152 kJ/mol [27].)

Dislocations formed during pre-deformation will provide heterogeneous nucleation sites for precipitation [28,29,30,31], hence precipitation will generally be facilitated by deformation. In order to determine the relation between $k_{0,S}(\varepsilon)$ / $k_{0,\beta}(\varepsilon)$ and ε, we propose a model based on the following assumptions:

- All dislocations are potential nucleation sites for S and β″ phases;
- Both the number of S phase nuclei, N_S, and the number of β″ phase nuclei, N_β, are proportional to the initial dislocation density, ρ_o, at the start of ageing;
- The pre-exponential factors $k_{0,S}(\varepsilon)$ and $k_{0,\beta}(\varepsilon)$ are proportional to the number of nuclei.

These assumptions lead to the following proportionality:

$$k_{0,i}(\varepsilon) \propto N_i \propto \rho_0 \qquad (i = S, \beta) \tag{4}$$

Meanwhile, the following relation exists [32,33]:

$$\Delta\tau_d^0 = \alpha_\rho G b \rho_0^{1/2} \tag{5}$$

where α_p is a unitless constant, it is here taken as 0.3. So, the initial dislocation density ρ_o is proportional to the square of the critical resolved shear stress (CRSS) increment due to dislocation strengthening, $\Delta\tau_d^0$, at work hardening state, i.e.,

$$\rho_0 \propto (\Delta\tau_d^0)^2 \tag{6}$$

As to be discussed below (in the work hardening model), the following relation exists:

$$\Delta\sigma_d^0 = M\Delta\tau_d^0 = K_{wh}\varepsilon^{n_{wh}} \tag{7}$$

where $\Delta\sigma_d^0$ is the stress contribution due to dislocation strengthening, and M is the factor describing the proportionality between yield strength and critical resolved shear stress of grains, which is often termed the Taylor factor. Thus the latter two equations provide the following proportionality:

$$\rho_0 \propto (\varepsilon)^{2n_{wh}} \tag{8}$$

Thereby, it also holds that $k_{0,i}(\varepsilon) \propto (\varepsilon)^{2n_{wh}}$ and thus we may write:

$$k_{0,i}(\varepsilon) = k_{\varepsilon,i}\varepsilon^{2n_{wh}} + k_{ND,i} \quad (i = S, \beta) \tag{9}$$

where k_τ and k_{ND} are constants.

This relation can be investigated using DSC data. For cold-rolled alloy A9, for all three reductions (10%, 40% and 90%), DSC data (see Fig. 4) show a clearly defined exothermic precipitation effect in the temperature range up to 300°C during DSC runs. TEM data (see below) indicates this is due to S phase formation. Using the concept of equivalent time (see Ref. [10]), the temperature to reach a particular stage (e.g. peak temperature T_p) in the formation of a phase at constant heating rate can be converted to a time (i.e. equivalent time t_p) to reach the same stage at an isothermal temperature. (Due to absence of dislocations which are nucleation sites for S phase, a different precipitation sequence to that for cold worked samples may occur for the solution treated samples. Therefore, the solution treated condition will not be considered here.)

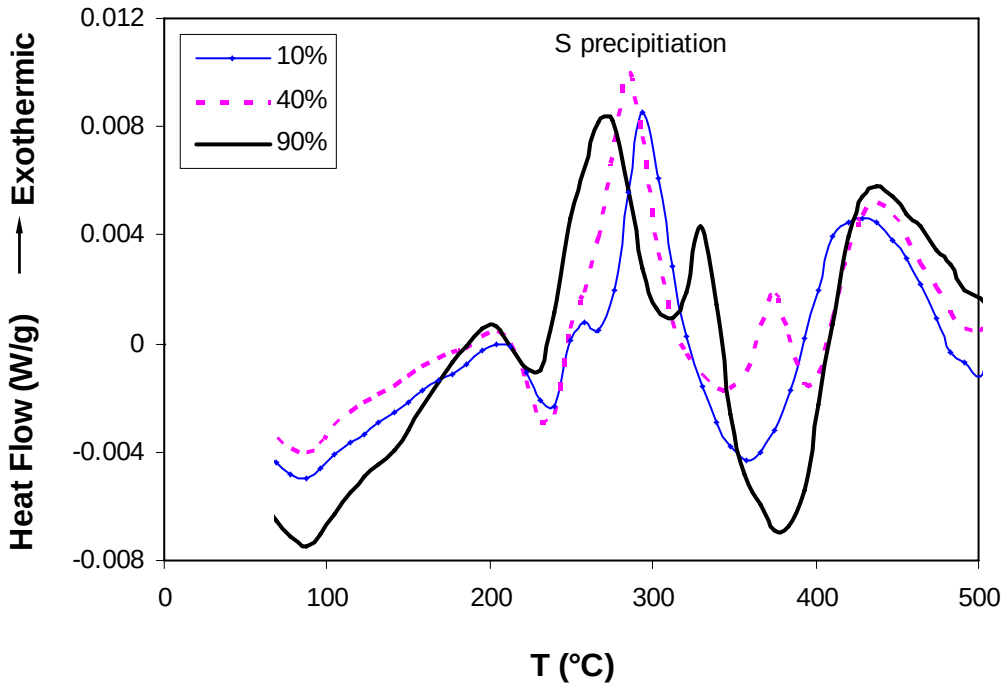

Fig. 4 DCS data for cold rolled alloy A9.

From the DSC data in Fig. 4, T_p is 294.9, 286.4 and 271.8°C for 10%, 40% and 90% reductions, respectively. The values of t_p obtained from the equivalent time equation in [10] are shown in Fig. 5. The model as introduced in this work (specifically Eqs. 2 and 9) would indicate that $1/t_p$ depends on ε in the following fashion:

$$1/t_p(\varepsilon) = g_1\varepsilon^{2n_{wh}} + g_2 \tag{10}$$

where g_1 and g_2 are constants and n_{wh} is the work hardening exponent, which is obtained from work hardening model (see below), and hence its value is fixed.. The fit of the latter equation to the limited number of available $1/t_p$ values shown in Fig. 5 reveals a fair correspondence, which indicates that the present treatment provides a reasonable description of the influence of cold work on precipitation rate. (But it should be noted that more work is needed to assess whether, within the current framework, an improved treatment can be effective.) In a similar treatment the relation between cold work and rate of formation of β″ phase was determined using DSC data for alloy A1.

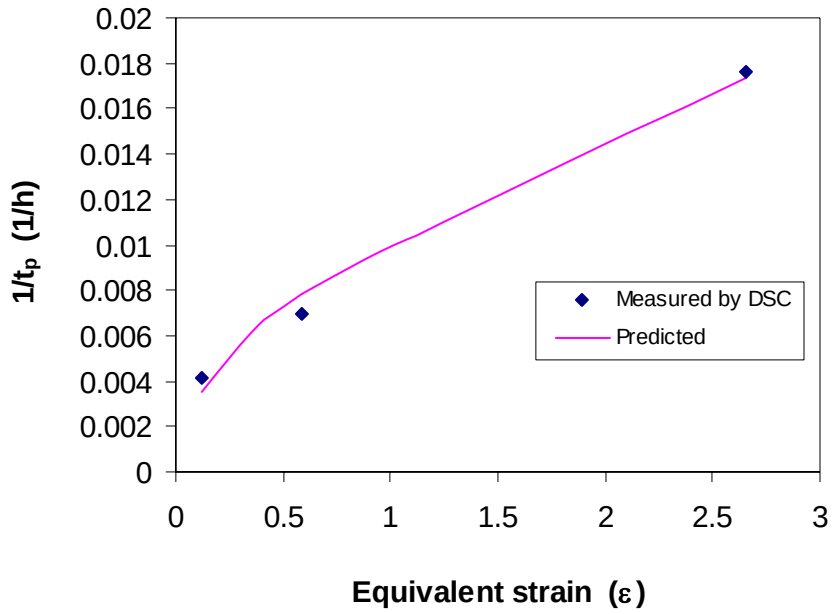

Fig. 5 Measured and fitted $1/t_p$ for alloy A9.

Conversion between atomic and volume fractions of precipitates can be performed when their composition and respective atomic densities, V_{at}^{S} and $V_{at}^{\beta''}$, are known. From the respective crystal structures, it can be shown that $V_{at}^{S} \cong V_{at}^{m}$ [27]. Therefore, for S phase, the volume fraction, f_s can be readily approximated by its atomic fraction, x_s, i.e., $f_S \cong x_S$. For β″ phase different crystal structures have been reported in the literature. The crystal structure of β″ phase was generally reported to be monoclinic, however, varying sets of lattice parameters have been reported [34]. In a simplified treatment, it can be shown that the average atomic diameter of the atoms in β″ is nearly identical to that of the Al-rich phase. Therefore, $V_{at}^{\beta''} \cong V_{at}^{m}$ thus we can approximate $f_{\beta''} \cong x_{\beta''}$.

Kinetic model: precipitate sizes

In the present model, a simple analytical approach proposed before [12,14] is applied to model the average size of the precipitates. In this approach we assume that new nuclei grow in three dimensions and retain their initial shape, and as a consequence the average size of precipitates in a particular direction during the nucleation and growth stage, $\bar{l}_g$, grows according to [12,14]:

$$\bar{l}_{g,i}(t) = \bar{l}_{0,i}\alpha_i^{1/3} \quad (i = S, \beta) \tag{11}$$

where $\bar{l}_0$ is the average precipitate size at the start of coarsening, and the subscripts S and β stand for phase S and β″, respectively. Assuming that the coarsening of the precipitates complies with the classical Lifshitz-Slyozov-Wagner (LSW) coarsening theory, the average size during the coarsening stage, $\bar{l}_c$, is given by:

$$[\bar{l}_{c,i}(t)]^3 = (\bar{l}_{0,i})^3 + k_{c,i}(T,\varepsilon)t \qquad (i = S, \beta) \tag{12}$$

where

$$k_{c,i}(T,\varepsilon) = k_{c0,i}(\varepsilon)\exp\left(-\frac{E^i_{co}}{RT}\right) \qquad (i = S, \beta) \tag{13}$$

where E_{co} is the activation energy for coarsening. To limit the number of fitting parameters in the model, the activation energy for coarsening is taken identical to the activation energy for precipitation, that is, $E^i_{co} = E^i_{ppt}$ is used throughout the model; k_{c0} is a pre-exponential factor depending on pre-strain, ε. It is assumed to have a similar dependence on strain as $k_0(\varepsilon)$ does and hence it follows:

$$k_{c0,i}(\varepsilon) = p_{k,i}k_{0,i}(\varepsilon) \qquad (i = S, \beta) \tag{14}$$

where p_k is a constant, subscripts S and β stand for S and β″ phases, respectively. The full evolution of size from nucleation through growth to coarsening, is captured by [12,14]:

$$\bar{l}_i(t) = \bar{l}_{g,i}(t) + \bar{l}_{c,i}(t) - \bar{l}_{0,i} \qquad (i = S, \beta) \tag{15}$$

4.2 Dislocation evolution model

Dislocation evolution of the cold worked samples during ageing involves dislocation generation due to work hardening during cold deformation, and dislocation annihilation due to recovery during ageing. In this section, models for dislocation generation and dislocation annihilation will be proposed to describe dislocation evolution during isothermal ageing.

Dislocation generation: work hardening model

In the modelling we will assume there is a direct relation between an average dislocation density and strengthening due to deformation. In this section, several work hardening models compatible with this assumption will be used to fit the experimental data on yield strength of cold worked samples. The model which gives the best fit will be selected.

Three types of stress-strain relations (work hardening) that can be represented in analytical equations were considered. These three types of stress-strain relation are:

- The Hollomon equation, which is a simple power law equation expressed as

$$\Delta\sigma_{wh} = K_{wh,H}\,\varepsilon^{n_{wh}} \tag{16}$$

where $K_{\mathrm{wh,H}}$ is the (Hollomon) strength coefficient, n_{wh} is the strain hardening exponent and ε is the von Mises equivalent strain in the case of cold rolling processing.

- The Voce equation, which is expressed as (see e.g. [35])

$$\Delta\sigma_{wh} = K_{wh,V}[1-\exp(-\frac{\varepsilon-\varepsilon_1}{\varepsilon_c})] \tag{17}$$

Where $K_{\mathrm{wh,V}}$ is a constant, ε_1 represent the initial stress and strain at the start of the deformation, ε_{c} is a characteristic strain for the material.

- A modified Voce equation, which is given by [36]

$$\Delta\sigma_{wh} = K_{wh,MV}\,\exp(n_v\varepsilon^{n_{wh}}) \tag{18}$$

where n_{wh} is a constant and $K_{\mathrm{wh,MV}}$ is a constant,.

ε_1 in the Voce equation is generally set as zero, and hence the above two equations can be rewritten as

$$\Delta\sigma_{wh} = K_{wh,MV}[1-\exp(n_v\varepsilon^{n_{wh}})] \tag{19}$$

When $n_{wh}=1$, the above equation reduces to the Voce equation. If $n_{wh}\neq 1$, it is equivalent to the modified Voce equation.

Analysis of the $\sigma_{0.2}$ data for our alloys in as quenched and cold-rolled conditions (i.e. 0, 10%, 40% and 90% cold work) showed that the work hardening rate increases with Mg and Cu concentrations. Through quantitatively analysing these yield strength data, the following relation between K_{wh} (for each of the models) and alloying contents was obtained:

$$K_{wh} = K_{wh}^{Mg}c_{Mg} + K_{wh}^{Cu}c_{cu} + K_{wh}^{0} \tag{20}$$

where K_{wh}^{Mg}, K_{wh}^{Cu} and K_{wh}^{0} are constants. This treatment of composition dependency of work hardening provides good model results (see below) and hence there is no evidence for composition dependency of n_{wh} in our data. We also want to limit the complexity of the model wherever possible, and thus n_{wh} is considered to be a single (fittable) parameter independent of composition.

Replacing K_{wh} in Eqs. 16 and 19 with the above equation and taking n_{wh} to be independent of alloy composition, the $\sigma_{0.2}$ data of the cold worked samples of the nine alloys were fitted. The obtained root mean squared errors (RMSEs) are 5.6 MPa, 22.0 MPa and 4.8 MPa for the Hollomon equation Eq. 16, Voce equation, Eq. 19 with $n_{wh}=1$ and modified Voce equation, Eq. 19 with $n_{wh}\neq 1$, respectively. Thus the Hollomon equation and the modified Voce equation give similar good accuracy for the available experimental data. (The difference in RMSE is much smaller than the experimental accuracy for determining $\sigma_{0.2}$). Hence, either can be used to describe the work hardening behaviour of the cold worked alloys. In this study, the Hollomon equation will be used as that is the more commonly employed equation.

In the following section, a one-parameter dislocation strengthening model will be applied. According to the one-parameter dislocation strengthening theory, $\Delta\sigma_{wh}$ can be given by the following equation:

$$\Delta\sigma_{wh}=\Delta\sigma_d^0=M\Delta\tau_d^0=M\alpha_\rho Gb\sqrt{\rho_0} \tag{21}$$

where the superscript 0 stands for t=0, i.e. the condition in the as cold-worked state, before artificial ageing is conducted. Therefore the dislocation density in the as cold-worked state, ρ_0, can be obtained from Eqs. 16 and 21 as:

$$\rho_0=\left(\frac{K_{wh}\varepsilon^{n_{wh}}}{M\alpha_\rho Gb}\right)^2 \tag{22}$$

Dislocation annihilation: recovery model

Based on a detailed survey on the experimental evidence and theoretical insights regarding recovery, Nes [37] found that the fraction residual strain hardening, R_{ReX}, can be commonly presented in terms of a logarithmic time decay law as follows [37]:

$$R_{\mathrm{Re}X}=\frac{\sigma(t)-\sigma_{\mathrm{Re}X}}{\sigma(t=0)-\sigma_{\mathrm{Re}X}}=1-S_{th}(T,\varepsilon)\ln[1+\frac{t}{t_r(T,\varepsilon)}] \tag{23}$$

This recovery time law was widely observed for a range of metals, including various cold rolled Al-Mg alloys with low to very high cold work levels [37,38]. $S_{th}(T,\varepsilon)$ and $t_r(T,\varepsilon)$ depend on the rate-controlling recovery mechanisms, which include thermally activated glide and solute drag [37]. In the present model, the recovery mechanism in the alloys isothermally aged at 170°C is assumed to be thermally activated glide. Following Ref. [37], S_{th} and the relaxation time t_p can be expressed as follows:

$$S_{th}=p_1T\frac{\sqrt{\rho_0}}{\sigma_{wh}-\sigma_{\mathrm{Re}X}} \tag{24}$$

$$t_r = [p_2\sqrt{\rho_0}\exp(\frac{p_3}{k_B T})]^{-1} \tag{25}$$

where p_1, p_2 and p_3 are constants, k_B is Boltzmann's constant.
For constant temperature experiments, S_{th} and t_p can be simplified as:

$$S_{th} = p_1^{'}\frac{\sqrt{\rho_0}}{\sigma_{wh} - \sigma_{\mathrm{Re}X}} \tag{26}$$

$$t_r = (p_2^{'}\sqrt{\rho_0})^{-1} \tag{27}$$

Meanwhile, the following proportional relation exists according to the work hardening model:

$$\sqrt{\rho_0} \propto \Delta\tau_d^0 \propto (\sigma_{wh} - \sigma_{rex}) \tag{28}$$

and thus, the following simplified expressions can be obtained at constant temperature:

$$S_{th} = p_1^{''} \tag{29}$$

$$t_r = p_2^{''}(\sigma_{wh} - \sigma_{\mathrm{Re}X})^{-1} \tag{30}$$

$\sigma_{\mathrm{Re}X}$ and σ_{wh} can be determined from the solution strengthening model and work hardening model, respectively, and hence $R_{\mathrm{Re}X}$ can be predicted by combining Eqs. 23, 29 and 30 On the other hand, the following derivation can be obtained in the absence of precipitation:

$$R_{\mathrm{Re}X} = \frac{\sigma_{rec}(t) - \sigma_{\mathrm{Re}X}}{\sigma_{wh} - \sigma_{\mathrm{Re}X}} = \frac{M\alpha_\rho Gb\sqrt{\rho(t)}}{M\alpha_\rho Gb\sqrt{\rho_0}} = \sqrt{\frac{\rho(t)}{\rho_0}} \tag{31}$$

where $\sigma_{rec}(t)$ and $\rho(t)$ are the yield strength and the dislocation density during recovery in the absence of precipitation, respectively. Hence the dislocation density evolution during the recovery process can be given by

$$\rho(t) = \rho_0(R_{\mathrm{Re}X})^2 \tag{32}$$

Subsequently, the dislocation strengthening contribution during recovery (i.e. the strength contribution due to stored dislocations initially generated by the cold-rolling) can be obtained by applying Eq. 5 which provides:

$$\Delta\tau_d(t) = \alpha_\rho Gb\sqrt{\rho(t)} = R_{\mathrm{Re}X}\Delta\tau_d^0 \tag{33}$$

4.3 Strengthening model

In order to model the yield strength of these cold-worked-and-aged alloys, the following contributions have to be considered in the yield strength model:

- Solid-solution strengthening, which is mainly due to Mg and Cu, $\Delta\tau_{ss}$
- Dislocation strengthening, i.e. work hardening and recovery, $\Delta\tau_{d}$
- Precipitation hardening, $\Delta\tau_{ppt}$
- Intrinsic resistance to shear of grains, $\Delta\tau_{0}$
- Grain boundary strengthening, $\Delta\sigma_{gb}$

All these contributions are considered, and they will be discussed in detail in this section.

Solid-solution hardening

Solid solution strengthening in these alloys was analysed before [5]. It was shown that the following treatment is highly accurate:

$$\Delta\tau_{ss} = \sum k_j c_j^{n_{ss}} \tag{34}$$

where k_j is a constant related to the properties of the related solute j. Theoretical treatments indicate n_{ss} could equal 2/3, 1 or ½, but our data indicates that for the present alloys n_{ss} =1 [5].

Dislocation strengthening

The dislocation evolution model in Section 4.2 is essentially a one parameter dislocation evolution model, i.e. it is based on an average dislocation density. It is derived using observations on yield strength evolution and the proportionality of strength increment (Eq. 21) with the root of the dislocation density as an integral part of its derivation. Thus strengthening due to dislocations is given by Eq. 33.

Precipitation hardening

Both S and β″ precipitates have a high aspect ratio (S precipitates are generally rod/lath-shaped particles, whilst β″ precipitates are generally reported to be needle/lath-shaped). Following studies on S phase strengthened [11] and β″ strengthened alloys [39], both are considered to be non-shearable. The contribution of the precipitates to strengthening can be evaluated by the following equation [40]:

$$\Delta\tau_i = \frac{0.81Gb}{2\pi(1-\upsilon)^{1/2}}\left(\frac{\ln(d_i/b)}{0.615d_i\sqrt{2\pi/3f_i}-d_i}\right) \qquad (i=S,\beta) \tag{35}$$

where υ is the Poisson's ratio for Al, d and f are the equivalent diameter and the volume fraction of the precipitates, respectively. Linear addition of strengthening contributions due do two classes of strengthening objects are appropriate when they have a strength that is different by at least an order of magnitude. But the obstacle strength of S and β″ precipitates to dislocation movements should be

of the same order of magnitude, because their sizes and shapes are similar (compare data in [11,25,41], and see Section 6) and the way they interact with dislocations is the same (they are both considered non-shearable). As the obstacle strength of S and β″ precipitates to dislocation movements should be of the same order of magnitude, we used the phenomenological quadratic superposition approximation which is considered to be a good approximation for obstacles of similar strength [5,40,42,43]:

$$(\Delta\tau_{ppt})^2 = (\Delta\tau_S)^2 + (\Delta\tau_\beta)^2 \tag{36}$$

Combined yield strength model

The superposition of the various contributions to the critical resolved stress provides the following equation for the yield strength [14,15,25,44]:

$$\sigma_y = \Delta\sigma_{gb} + M\ \tau_{tot} = \Delta\sigma_{gb} + M\,[\Delta\tau_0 + \Delta\tau_{ss} + (\Delta\tau_d^2 + \Delta\tau_{ppt}^2)^{1/2}] \tag{37}$$

For completeness the grain boundary strengthening term, $\Delta\sigma_{gb}$, is included. However, we will here neglect grain boundary strengthening as the grain sizes of the alloys are too large to provide significant grain boundary strengthening. Within Eq. 37 a superposition rule for $\Delta\tau_d$ and $\Delta\tau_{ppt}$ is applied. This is required because these two contributions are of a similar magnitude and similar to Eq. 36 we used the phenomenological quadratic superposition approximation which is considered to be a good approximation for obstacles of similar magnitude. (A further issue that may be noted here is that a further interaction occurs when precipitates form on part of the dislocation. In this case that section of the dislocation essentially disappears in terms of a contribution to strengthening. We here consider that this effect is negligible.)

5 Calibration and testing of the model

A key stage of the work is the calibration and testing of the model. The procedure followed here is inspired by the recognizing two main principles of calibration and testing. Firstly, the most objective way of testing any model is by comparing model predictions with "unseen" data, i.e. data that has not been used in deriving any element of the model or parameters within it [14]. The relative success (or failure) of the model then needs to judged from a measure of the average deviation between predicted values and measured unseen values; the measure usually taken for this is the average of the squares of the deviation (the mean-squared error, MSE) or its root (the root-mean-square-error, RMSE). Secondly, we need to recognize that the values of several of the parameters in the model are not known, or only approximately known. These two principles have a general validity in any attempt of devising models which aim to have predictive capabilities. In this section, the methods used to calibrate and test the model will be described in detail.

In calibrating the model the first step is by adopting the values for the parameters that were given in the in the previous section and parameters that are well known for the present alloys (e.g. b, G). All these parameters which are fixed in the calibration and testing procedure are shown in Table 2. Next we take the parameters for solution strengthening from an analysis of data from solutionised alloys which was presented in a previous paper [5]. The remaining parameters will be determined through model calibration. In principle, a range of procedures for calibrating and testing can be devised. One can use subsets of the available data to derive values for individual parameters and continue this in a step by step process (see e.g. [45]). However, in terms of computing time and deriving the true accuracy of the model it is preferred to fit the parameters to a randomised sample of the data and subsequently verify accuracy by checking predictions against the remaining "unseen" data [14]. Thus the proof strength data will be separated into two parts and only part of tensile data (about 50%) will be used for calibration ("training") of the model, the remaining tensile data will be used for testing the model, to derive a true accuracy for the predictive capability of the model (i.e. for unseen data). We will however make one limited modification to this method. As the available experimental tensile test data gathered in this study can not provide enough information to determine peak ageing time (the ageing times are too far apart to accurately determine a time to peak age), the parameters $k_{\varepsilon,\beta}$ and $k_{\varepsilon,S}$ will be determined from the hardness data (Fig. 1). (I.e. $k_{\varepsilon,\beta}$ and $k_{\varepsilon,S}$ are chosen such that the time to predicted peak proof strength coincides with peak hardness.)

Table 2 Fixed parameters used in the model

Parametes	Value	
ΔS_β	7.1×10^5	(calculated from Ref[41])
ΔS_S	5.0×10^5	(from Ref[27])
ΔH_β	95.9 kJ/mol	(from Ref[41])
ΔH_S	77.0 kJ/mol	(from Ref[27])
α_p	0.3	
G	27 GPa	
b	0.286 nm	
υ	0.33	
M	2.6	
n_s, n_β	2.5	(from Ref[10])
η	1	(from Ref[10])
E^β_{ppt}, E^S_{ppt}, E^β_{co}, E^S_{co}	152 kJ/mol	
k_{Mg}	590 MPa	(from Ref[5])
$\Delta\tau_0$	10 MPa	(evaluated from yield strength of pure aluminium)

The above described calibration and testing scheme was performed, and a model is obtained. A plot of predicted vs. measured proof stress is presented in Fig. 6 and the predictions of individual alloy and cold working reduction are shown in Fig. 2 together with the measured results. The parameters determined by fitting the model to a set of randomly selected data are presented in Table 3. (Small variations of some parameters may be obtained when a different set of data is selected for training the model. However, the model accuracy is not significantly affected by these variations.) The training and testing procedure provides an average RMSE on unseen data of 8.6 MPa. With the range of strength values of 240MPa this equates to a modelling accuracy of about 3.6%. We believe this percentage accuracy is far better (by at least a factor 2) than the accuracy of any previously reported physically based model for strength of a range of alloys, whether reported as a numerical value for model accuracy or implied by graphs of model predictions with data.

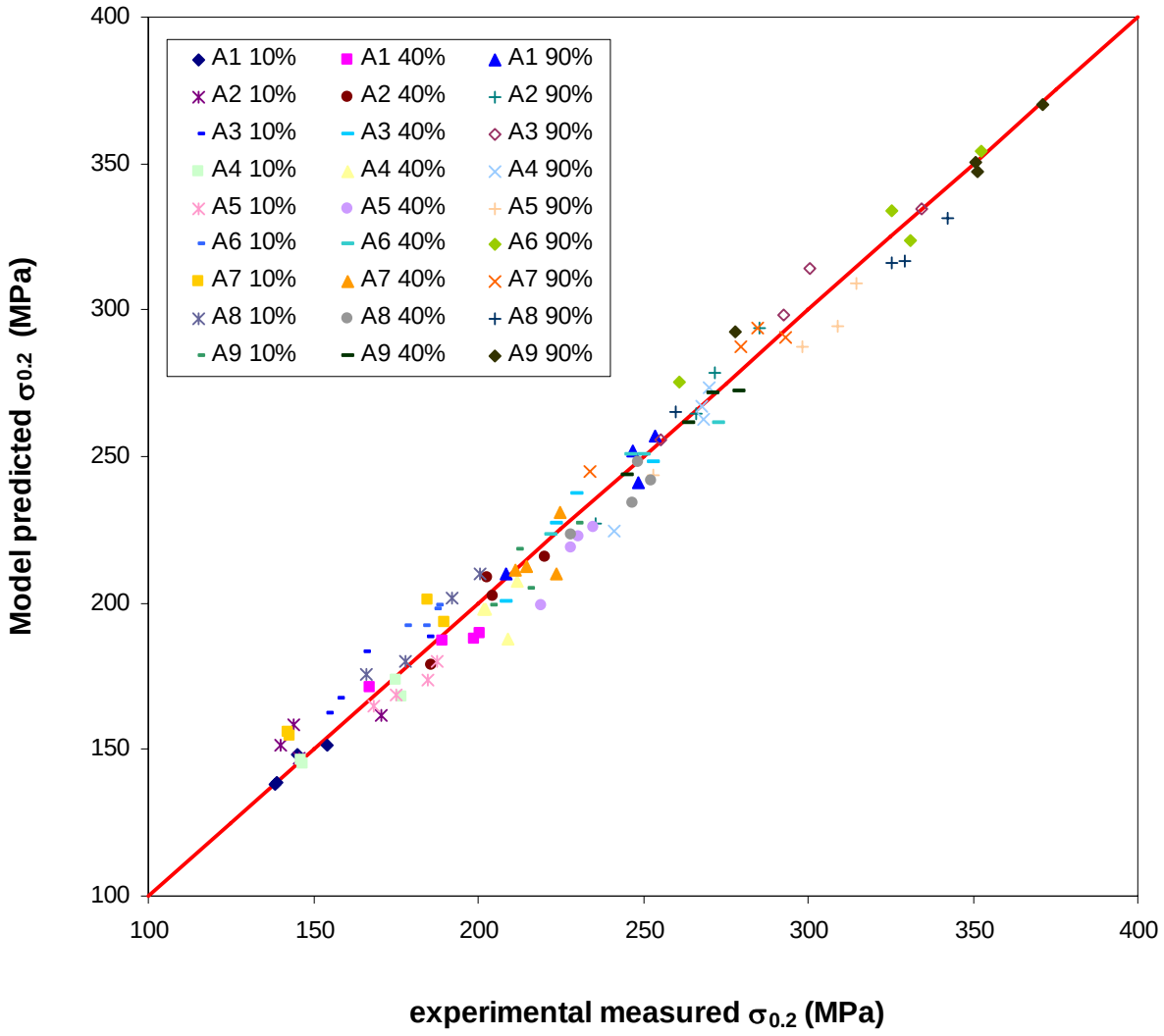

Fig. 6 Predicted $\sigma_{0.2}$ vs. measured $\sigma_{0.2}$.

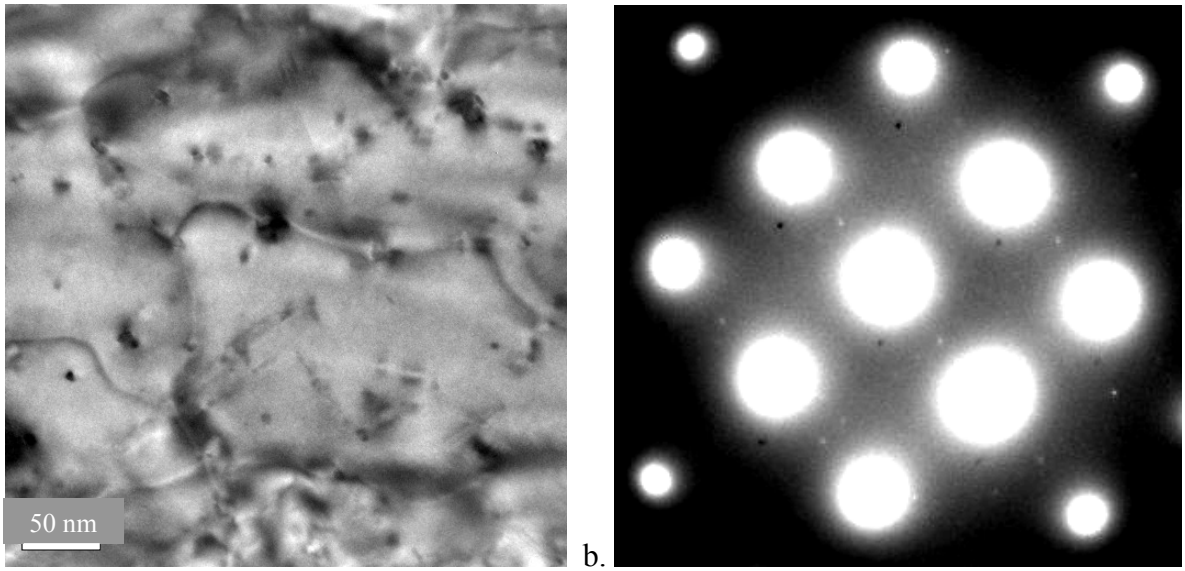

Fig. 7 TEM results of alloy A1 cold rolled at 10% reduction and subsequently aged 3 weeks at 170ºC: a. BF image at [100] zone axis, b. corresponding SAD.

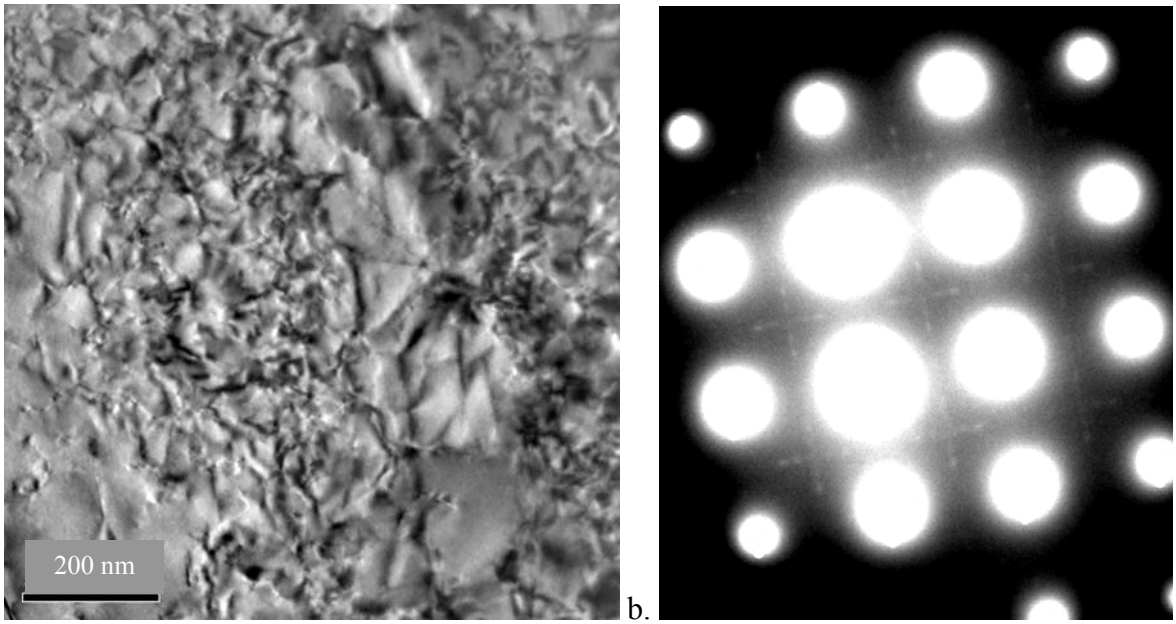

Fig. 8 TEM results of alloy A9 cold rolled at 10% reduction and subsequently aged 5 days at 170ºC: a. BF image at [100] zone axis, b. corresponding SAD.

Detailed, point by point examination of deviations between measured and predicted data in Fig. 2 and Fig. 6, and their correlations, was performed. It is thought that any remaining deviation can be explained mostly by: (i) random variations due to slight deviations in the actual cold rolling reduction achieved (i.e. in Fig. 2 a set of data points for one alloy at a single rolling reduction may have deviations that are offset with regards to predicted ageing curve) and (ii) random variations in each point, presumably due to slight measurement errors and small model inaccuracies. There is no evidence for a systematic source of error / deviations.

Table 3 Determined values for fitting parameters used in the model

Parameter		Value
work hardening	K_{wh}^{Mg}	1.69 GPa
	K_{wh}^{Cu}	15.1 GPa
	K_{wh}^{0}	0.14 GPa
	n_{wh}	0.275
recovery	p''_1	0.035
	p''_2	53.8 s.GPa
β'' precipitation	$k_{\varepsilon,\beta}$	4.0×10^{14} 1/s
	$k_{ND,\beta}$	5.0×10^{8} 1/s
	$l_{0,\beta}$	5.9 nm
	$p_{k,\beta}$	0.1
S precipitation	$k_{\varepsilon,s}$	7.5×10^{13} 1/s
	$k_{ND,s}$	5.0×10^{8} 1/s
	$l_{0,s}$	4.8 nm
	$p_{k,s}$	0.8

6 Discussion

Having successfully calibrated the model and tested its accuracy in predicting yield strength data, we next want to verify to what extend the calibrated parameters are consistent with the physics in the model and any relevant literature data (on microstructure, thermodynamics, or otherwise) that is available. In this section we will consider available microstructure data.

In accordance with experimental data, the model predicts that the precipitation hardening due to β″ phase formation decreases with increasing Mg content. According the model prediction, this is attributed to the formation of non-soluble Mg_2Si particles during solution treatment at 500°C. The model predicts that the higher the Mg content in the alloy, the higher the amount of Mg_2Si particles formed during solutionising at 500°C. This prediction agrees well with the results of the SEM/EDS intermetallics examinations of the present alloys [5].

The predicted precipitation in the Cu-free Al-Mg alloys with small Si additions can also be supported by TEM results. As shown in Fig. 7, the bright field (BF) image of a sample of 10% cold worked alloy A1 subsequently aged 3 weeks at 170°C shows some precipitates, and the corresponding selected area diffraction (SAD) shows faint additional reflections from the precipitates, which are consistent with diffraction patterns of β' phase. The model also predicts that, in the Cu-containing alloys with 3wt% Mg (i.e., alloys A6 and A9), S phase is the main strengthening phase because most of the Si is removed from the solid solution due to the formation

of Mg_2Si particles during solutionising and hence little Si is available for precipitation during subsequent ageing. This prediction is also supported by TEM experiments. TEM results for 10% cold worked alloy A9, subsequently aged 5 days at 170°C, show a high density of dislocations and no precipitates could be unambiguously identified in the BF image (Fig. 8a). However, the SAD (Fig. 8b) shows a pattern consistent with S phase. These observations support the model.

It should be noted that microstructure study by TEM observations for these cold-rolled and aged samples is difficult. Compared with typical heat treatable alloys, e.g., 2XXX, 6XXX and 7XXX, the volume fraction of precipitates in all alloys studied is very small. Combined with the very high density of dislocations (due to heavy cold work), this makes the identification of precipitates very difficult. In several cases TEM and SAD investigations proved inconclusive as to the presence of precipitates, even though DSC experiments had indicated formation of precipitates. An investigation of the dislocation densities in the cold-rolled plates shows a good agreement with dislocation densities predicted in the model [9].

The size of precipitates at the start of coarsening has a strong influence on the peak strength of the alloys during ageing [14,15,45]. In a slightly overaged AA2024 (Al-4wt%Cu-1.5wt%Mg) sample, the measured radii of the S rods from the edge on variants range from about 2.5 nm to 6 nm with an average of 4.4 nm [46] and in models for evolution of $\sigma_{0.2}$ during ageing, $l_{0,S} = 4.7$ nm provides a best fit for Al-Cu-Mg alloys [11,25] with Cu contents above 1wt%. Analysis of TEM data on an Al-Mg-Si alloy published by Myhr et al [41], shows that the mean precipitate radius in terms of an equivalent radius of sphere with identical volume is about 4.9±1.5. The calibrated values for $l_{0,\beta}$ and $l_{0,S}$ in our model (5.9 nm and 4.8 nm), are quite close to these experimental values, which indicates that this aspect of the model (size of precipitates, and by extension the strengthening contribution by the precipitates) is sound.

At this point it is valuable to note that the procedure for calibration of parameters can be further analysed to check the level of sensitivity of model predictions to the value for the parameters. And, vice-versa, the procedure for calibration of parameter yields values for the parameters which will have their own level of reliability, with parameters to which the model predictions are less sensitive being determined with a more limited accuracy. With this in mind, it is useful to consider perform an alternative calibration of the model, in which the values of $l_{0,\beta}$ and $l_{0,S}$ are fixed to the values suggested from the above mentioned literature data (in [11,25,41]), 4.9 nm and 4.7 nm, respectively. In this alternative calibration the overall test accuracy of the model changes very little: less than 0.5MPa. These observations on measured and fitted $l_{0,\beta}$ and $l_{0,S}$ show two main points: i) the accuracy in $l_{0,\beta}$ and $l_{0,S}$ determination through the calibration procedure is limited to about 20% ii) the treatment of precipitation hardening in the model is fully consistent with published TEM observations on the sizes of S and β″ precipitates.

$k_{c,i}(T,\varepsilon)$ ($i = \beta,$ S) determines the coarsening rate of the precipitates, which can be determined by measuring the precipitate size at different times of coarsening stage using TEM. There are some limited literature data on the coarsening rate of S phase, which were reviewed in Ref. [47] (see Table I and Figure 1 in Ref. [47]). In non-stretched alloys, these measured data differ by quite a large magnitude (in one case up to 5 orders of magnitude) and none of these data were measured at or near 170°C, requiring significant extrapolation. Thus there will be a significant level of uncertainty in any attempt to compare our calibrated values of $k_{c,i}(T,\varepsilon)$ with literature data. Of the data available there are two independent data series (from Sen et al [48] and Cho [49]) which contain sufficient data points, with a consistent trend, that makes them suitable for extrapolation to our ageing temperature of 170°C. This extrapolation provides values of $k_{c,S}(T,\varepsilon = 0)$ at 170°C of 4.4×10^{-4} nm^{-3}/s and 1.7×10^{-4} nm^{-3}/s, respectively; and averaged value is 2.7×10^{-4} nm^{-3}/s with a standard deviation of about a factor 4 (i.e. $2.7^{+11}_{-2.1}\times10^{-4}$ nm^{-3}/s). The predicted values for $k_{c,S}(T,\varepsilon = 0)$ by our model are 0.24, 0.56 and 1.26×10^{-4} nm^{-3}/s for 10%, 40% and 90% pre-reduction, respectively. The level of correspondence is a borderline case, and highly reliant on extrapolation of data. Taking this into account and considering the influence of the dilute alloy composition and cold work in this study on the coarsening rate of precipitates, the predicted values in this study are thought to be very reasonable. No reliable data for $k_{c,\beta''}(T,\varepsilon)$ is available in the literature.

In the yield strength model, a quadratic superposition rule has been applied for the contributions of dislocation strengthening and precipitation hardening. As indicated (in Section 4), theory of strengthening due to multiple types of obstacle, indicates this type of superposition is appropriate. To test this theory, a linear superposition of the two contributions has also been attempted. After retraining the model, the accuracy of the model on unseen data is not significantly affected, but the fitted values for $l_{0,\beta}$ and $l_{0,S}$ parameters changed to 12.6 nm and 9.1 nm, respectively, both of which are much higher than the available literature data. These results are indicative of two main issues. Firstly, because $l_{0,\beta}$ and $l_{0,S}$ parameters required for an optimal fit are much higher than the direct observations in the available literature suggest, a linear superposition of the two contributions is inconsistent with the present data. Secondly, this test of a model variant indicates that whilst the present model has a very good accuracy, a slightly changed variant of the model can obtain similar model accuracy, which in turn suggests that further improvements in the description of precipitation hardening and superposition of different precipitation hardening contributions may be possible. Finding of this type tend to receive little or no mention in most published work, as critical comparisons of predictive accuracy of model variants are very rare. Nevertheless, the latter finding should not be surprising, because it is in fact quite clear that unless the model is very simple any quantitative model incorporating a range of different effects that is tested against data (which in itself will have limitations to its accuracy) can be modified to some small extend with resulting model accuracies seeing little change. Progress in modelling can only be achieved by critically testing models, within the context of the clear understanding that any materials model, by

definition, contains approximations. For all elements in the present model more refined treatments are possible. However, the present work shows that within the approximations applied a very efficient model with exceptionally high accuracy for prediction of unseen strength data for complex alloys can be derived.

8 Conclusions

The age hardening and age softening of nine solution treated and subsequently cold-rolled Al-(1-3)Mg-(0-0.4)Cu-0.15Si-0.25Mn (in wt%) alloys has been investigated. Solution treatment at 500°C and subsequent cold rolling with reduction of 10, 40 and 90% was conducted on all alloys. The work shows the following.

- A physically based model for yield strength has been developed. This model includes a one parameter dislocation evolution model to describe work hardening and recovery and a two precipitate precipitation hardening model. The model is based on analytical equations, avoiding computing time intensive iterative schemes.
- The model has been trained and subsequently tested using unseen data. An exceptionally high model accuracy of about 9 MPa (about 4% of the range of proof strength values) has been demonstrated. The model fits and explains all changes in strength and hardness well.
- All parameters in the model are within ranges that can be expected on the basis of microstructural investigations and literature data.
- The model results support the quadratic superposition rule for the contributions of dislocation strengthening and precipitation hardening.
- The cold worked Cu-containing alloys precipitation harden during ageing at 170°C. The main cause for this is S phase formation.
- For all three reductions, the Cu free Al-1Mg-0.15Si alloy (alloy A1) shows a distinct precipitation hardening effect. The hardness increases with cold rolling reduction, but on extensive ageing the differences in the hardness due to different cold-rolling reductions become smaller. Increasing the Mg content causes the age hardening effect to disappear. The model indicates that this is due to undissolved Mg_2Si.

Acknowledgements

The authors would like to thank Alcan International for providing the alloys and partial financial support for this work, and thank Drs G. Mahon (currently at Innoval, UK), M. Hao and S. Court (currently at NAMTEC, UK) for their technical input.

References

[1] J. Courbon, Scripta Mater. 48 (2003) 1519 -1524
[2] G.B.Burger, A.K. Gupta, P.W. Jeffrey, D.J. Lloyd, Mater. Charact. 35 (1995) 23
[3] S.A. Court, K.M. Gatenby, D.J, Lloyd, Mater. Sci. Eng. A 319 (2001) 443 -447
[4] P. Ratchev, B. Verlinden, P. De Smet, P. Van Houtte, Acta Metall. Mater. 46 (1998) 3523

[5] Z. Zhu M.J. Starink, Mater. Sci. Eng. A 488 (2008) 125-133
[6] B. Verlinden, A.-M. Zahra, Mater. Sci. Forum 426-432 (2003) 423
[7] M.J. Starink, J. Mater. Sci. 36 (2001) 4433-4441
[8] R. Kampmann, R. Wagner, in: P. Haasen, V. Gerold, R. Wagner, M.F. Ashby (Eds), Decomposition of Alloys: the Early Stages, Pergamon Press, New York, 1983, p. 91
[9] S.C. Wang, Z. Zhu, M.J. Starink, J. Microscopy 217 (2005) 174–178
[10] M.J. Starink, Int. Mater. Rev. 49 (2004) 191-226
[11] S.C. Wang, F. Lefebvre, J.L. Yan, I. Sinclair, M.J. Starink, Mater. Sci. Eng. A 431 (2006) 123-136
[12] M.J. Starink, Mater. Sci. Forum 539-543 (2007) 2365-2370
[13] M.J. Starink, N. Gao, L. Davin, J. Yan, A. Cerezo, Phil. Mag. 85 (2005) 1395-141
[14] M.J. Starink, S.C. Wang, Acta Mater. 51 (2003) 5131-5150
[15] I.N. Khan, M.J. Starink, Mater. Sci. Eng. A, in press
[16] M. J. Starink, A. Cerezo, J. Yan, N. Gao, Philosoph. Mag. Lett. 86 (2006) 243-252
[17] J. Buha, R.N. Lumley, A.G. Crosky, K. Hono, Acta Mater 55 (2007) 3015-3024
[18] M.A. van Huis, J.H. Chen, M.H.F. Sluiter, H.W. Zandbergen, Acta Mater 55 (2007) 2183-2199
[19] P. Donnadieu, G.F. Dirras, J. Douin, Mater Sci For 396 (2002) 1019
[20] S.C. Wang, M.J. Starink, N. Gao, Scr. Mater. 54 (2006) 287-291
[21] M.J. Starink, A. Dion, Thermochim. Acta 417 (2004) 5-11
[22] S.C. Wang, M.J. Starink, Int. Mater. Rev. 50 (2005) 193-215
[23] D.J. Chakrabarti, D.E. Laughlin, Prog. Mater. Sci. 49 (2002) 389-410
[24] M.J. Starink, A.-M. Zahra, Phil. Mag. A 76 (1997) 701-714
[25] M.J. Starink, J.L. Yan, Mater. Sci. Forum 519-521 (2006) 251-258
[26] M.J. Starink, Mater. Sci. Eng. A 276 (1999) 288-291
[27] J.L. Yan,. PhD thesis. School of Engineering Sciences, University of Southampton, 2006
[28] H.S. Zurob, Y. Brechet, G. Purdy, Acta Mater. 49 (2001) 4183
[29] H.S. Zurob, C.R. Hutchinson, Y. Brechet, G. Purdy, Acta Mater. 50 (2002) 3075
[30] M.J. Starink, P.J. Gregson, Mater. Sci. Eng. A 211 (1996) 54-65
[31] S.C. Wang, M.J. Starink, Acta Mater. 55 (2007) 933-941
[32] U.F Kocks, H. Mecking, Prog. Mater. Sci. 48 (2003) 171
[33] M.F. Ashby, Phil. Mag. 21 (1970) 399
[34] C. Ravi, C. Wolverton, Acta Mater. 52 (2004) 4213
[35] P.V. Sivaprasad, S. Venugopal, S. Venkadesan, Mater. Sci. Technol. 20 (2004) 350
[36] D.J. Lloyd, D. Kenny, Metall. Trans. A 13A (1982) 1445
[37] E. Nes, Acta Metall. Mater. 43 (1995) 2189
[38] D. Kuhlmann-Wilsdorf, Philos. Mag. A 79 (1999) 955
[39] G.F. Dirras, P. Donnadieu, J. Douin, Probl. Mater. Sci. 1 (2003) 33
[40] M.J. Starink, P. Wang, I., Sinclair, P.J. Gregson, Acta Mater. 47 (1999) 3855
[41] O.R. Myhr, O. Grong, S.J. Andersen, Acta Mater. 49 (2001) 65
[42] L.M. Brown, R.K. Ham, Dislocation-particle interactions, in Strengthening methods in crystals, A. Kelly, R.B. Nicholson (Eds), 1971, Elsevier: London. p. 9
[43] C. Schlesier, E. Nembach, Acta Metall. Mater. 43 (1995) 3983
[44] M.J. Starink , A. Deschamps, S.C. Wang, Scr. Mater. 58 (2008) 377-382
[45] H. R. Shercliff, M. F. Ashby, Acta Metall Mater, 38 (1990) 1803-1812
[46] M.J. Starink, J.-L. Yan, ASM Mater. Solution 2003. M. Tiryakioglu, L.A. Lalli (Eds), 2003. p. 119, Pittsburgh, Pennsylvania: ASM International
[47] W.M. Rainforth, H. Jones, J. Mater. Sci. Lett. 16 (1997) 420
[48] N. Sen, D.R.F. West, J. Inst. Met. 97 (1969) 87
[49] H.K. Cho, J. Korean Inst. Met. 16 (1978) 160